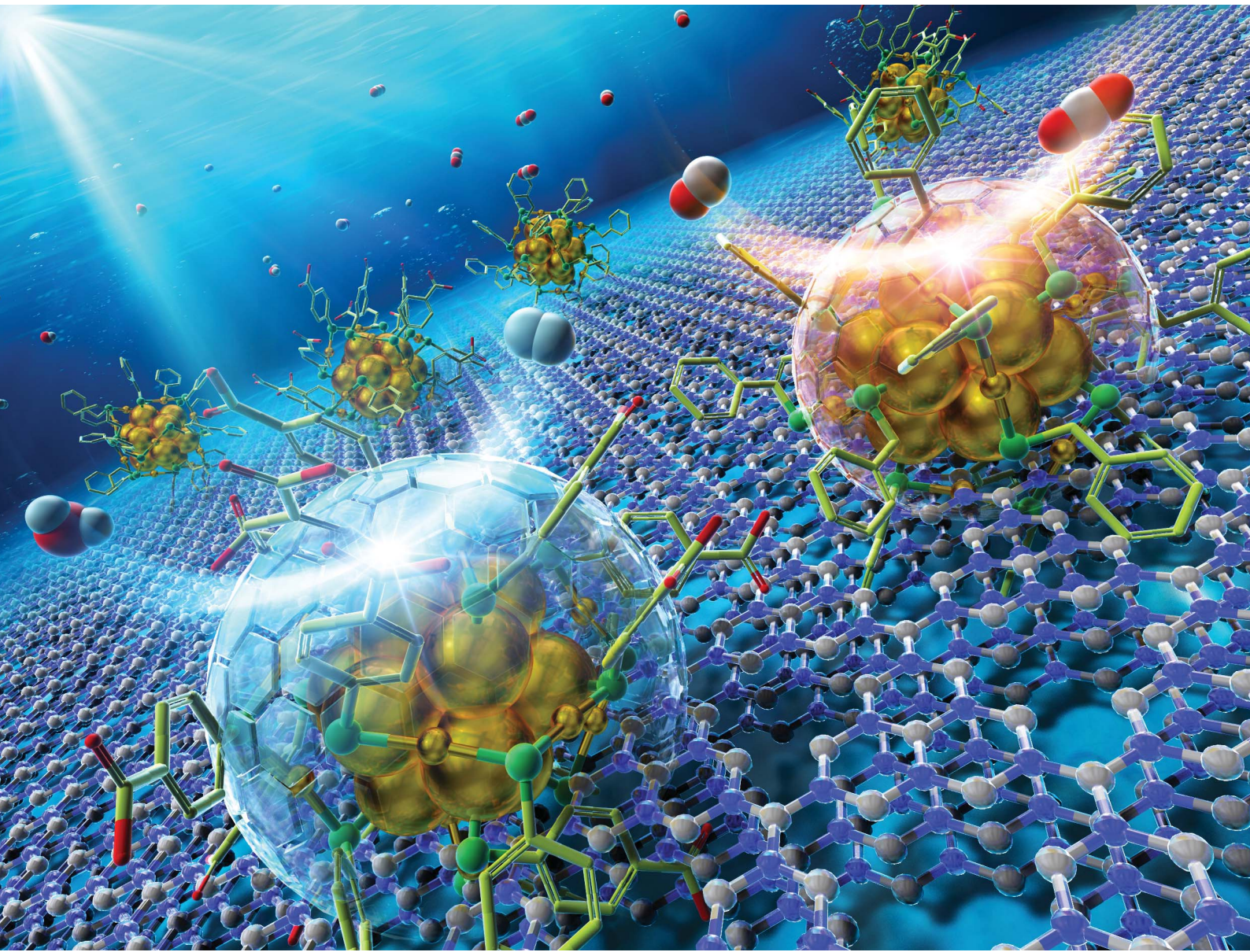


# Nanoscale Advances

[rsc.li/nanoscale-advances](http://rsc.li/nanoscale-advances)



ISSN 2516-0230



Cite this: *Nanoscale Adv.*, 2025, **7**, 1518

## Activation of photocatalytic $\text{CO}_2$ reduction by loading hydrophobic thiolate-protected $\text{Au}_{25}$ nanocluster cocatalyst†

Yuki Yamazaki,‡<sup>a</sup> Yuki Tomoyasu,‡<sup>a</sup> Tokuhisa Kawasaki  \*<sup>ab</sup> and Yuichi Negishi  \*<sup>bc</sup>

The photocatalytic carbon dioxide ( $\text{CO}_2$ ) reduction reaction ( $\text{CO}_2\text{RR}$ ), which reduces  $\text{CO}_2$  to various useful chemical compounds by light, has attracted attention to achieve carbon neutrality. In photocatalytic  $\text{CO}_2\text{RR}$ , it is effective to load metal nanoparticles (NP) as cocatalysts on the surface of semiconductor photocatalysts to improve their activity and selectivity. In this study, we used ultrafine metal nanoclusters (NC) with a particle size of about 1 nm as cocatalysts to clarify the effect of surface ligands on the activity and selectivity of the photocatalytic  $\text{CO}_2\text{RR}$ . As a result, it was shown that the introduction of hydrophobic ligands to the  $\text{Au}_{25}$  NC cocatalyst suppresses the competing hydrogen evolution reaction, thereby increasing the selectivity of  $\text{CO}_2\text{RR}$ . In addition, the hydrophobic ligand-protected  $\text{Au}_{25}$  NC cocatalysts exhibited 66 times higher CO evolution rates per Au-loading weights than the Au NP cocatalysts with a particle size of about 7 nm. These results provide crucial insights into the creation of highly active metal NC cocatalysts for photocatalytic  $\text{CO}_2\text{RR}$ .

Received 18th December 2024  
Accepted 11th February 2025

DOI: 10.1039/d4na01045k  
[rsc.li/nanoscale-advances](http://rsc.li/nanoscale-advances)

## Introduction

The photocatalytic carbon dioxide ( $\text{CO}_2$ ) reduction reaction ( $\text{CO}_2\text{RR}$ ), which reduces  $\text{CO}_2$  by light, is expected to be put to practical use as one of the means to solve energy, environmental and resource issues.<sup>1,2</sup> This is because if exceedingly stable  $\text{CO}_2$  can be converted into various useful chemical compounds using sunlight,  $\text{CO}_2$  can be recycled and we can break free from the conventional energy systems that rely on fossil resources. For the practical use of the photocatalytic  $\text{CO}_2\text{RR}$ , it is essential to further improve the efficiency and selectivity of the reduction products. Herein, commonly used photocatalysts are composed of a semiconductor photocatalyst and a metal/metal oxide cocatalyst. Importantly, many semiconductor photocatalysts that have a band gap suitable for  $\text{CO}_2\text{RR}$  have been developed, and visible-light-driven photocatalysts that can respond to visible light rather than only ultraviolet light have been actively investigated in recent years.<sup>3–7</sup> At the same time, the selection/

fabrication of appropriate cocatalyst nanoparticles (NP) that have a significant impact on their activity and selectivity have also been developed. For example, it has been reported that Ag and Au NP cocatalysts mainly produce CO,<sup>8–13</sup> whereas Pd, Cu and Rh–Ru alloy NP cocatalysts mainly produce  $\text{CH}_4$ .<sup>2,14–17</sup>

In addition, it is known that using smaller cocatalysts improves the activity of the catalytic reaction. In particular, when metal nanoclusters<sup>18–25</sup> (NC) with a particle size of about 1 nm are used as cocatalysts, their photocatalytic activity for water splitting is greatly improved.<sup>26–32</sup> This improvement is mainly due to (1) the increase in the number of active sites due to the increase in the specific surface area and (2) the optimization of the adsorption characteristics with the reaction substrates due to the change in the electronic state based on the quantum size effect. In general, the water splitting activity of metal NC cocatalysts for photocatalysts is improved when (i) their surfaces are protected by ligands with hydrophilic functional groups<sup>33</sup> or (ii) the hydrophobic ligands are removed.<sup>28,34</sup> This is because the presence of hydrophilic functional groups or removal of hydrophobic ligands makes it easier to be approached by protons ( $\text{H}^+$ ), which are the reaction substrate, on the surface metal atoms of the metal NC. By contrast, in photocatalytic  $\text{CO}_2\text{RR}$ , the hydrogen evolution reaction (HER) due to water splitting is a competitive reaction. Therefore, if such photocatalytic HER can be suppressed by enhancing the hydrophobicity of the surface ligands, high selectivity and activity for photocatalytic  $\text{CO}_2\text{RR}$  is expected to be obtained (Fig. 1A).

<sup>a</sup>Department of Applied Chemistry, Faculty of Science, Tokyo University of Science, 1-3 Kagurazaka, Shinjuku-ku, Tokyo 162-8601, Japan

<sup>b</sup>Carbon Value Research Center, Research Institute for Science & Technology, Tokyo University of Science, 2641 Yamazaki, Noda, Chiba 278-8510, Japan

<sup>c</sup>Institute of Multidisciplinary Research for Advanced Materials, Tohoku University, Katahira 2-1, Aobaku, Sendai 980-8577, Japan

† Electronic supplementary information (ESI) available: Experiment, characterization, additional figures, characterization of Au NC, additional UV-vis, XANES, FT-EXAFS, EXAFS spectra, TEM image and photocatalytic activity. See DOI: <https://doi.org/10.1039/d4na01045k>

‡ These authors contributed equally to this work.



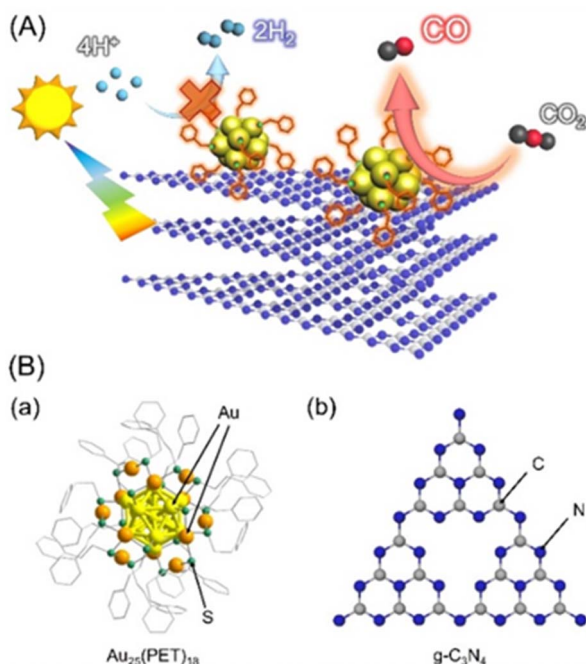


Fig. 1 (A) Schematic of the purposes of this study and (B) geometric structure of (a)  $\text{Au}_{25}(\text{PET})_{18}$  and (b) gCN photocatalysts.

In this study, we attempted to experimentally verify such an assumption regarding the effects of the functionality of ligands of metal NC on photocatalytic CO<sub>2</sub>RR activity. Specifically, we used  $\text{Au}_{25}$  NC<sup>35,36</sup> (Fig. 1B(a)), which are the most common model NC with high electrocatalytic CO<sub>2</sub>RR activity<sup>37–40</sup> as cocatalysts and attempted to clarify the effects of hydrophobic and hydrophilic ligands that protect them during photocatalytic CO<sub>2</sub>RR activity. As a result, it was shown that the introduction of hydrophobic ligand-protected  $\text{Au}_{25}$  NC cocatalyst suppressed the competing HER, thereby increasing the selectivity of the CO<sub>2</sub>RR and it exhibited 66 times higher CO evolution rates per Au-loading weight than the Au NP cocatalysts made by a conventional photodeposition (PD) method.

## Results and discussion

In this study, we used g-C<sub>3</sub>N<sub>4</sub> photocatalysts (gCN; Fig. 1B(b)), which have attracted much attention as a next-generation visible-light-driven photocatalyst because of their ease of synthesis, nontoxic nature, abundant availability of the raw materials on the Earth, and high physical and chemical stability.<sup>41–45</sup> There have also been many reports of gCN as a photocatalyst for photocatalytic CO<sub>2</sub>RR.<sup>46–48</sup> We synthesized gCN from urea by thermal polymerization as previously reported,<sup>29</sup> and measured the powder X-ray diffraction and diffuse reflectance (DR) spectrum of the obtained gCN. From these results, we confirmed that the synthesized photocatalyst was visible-light-responsive g-C<sub>3</sub>N<sub>4</sub> with relatively high crystallinity (Fig. S1†).

Next,  $\text{Au}_{25}$  NC protected by 2-phenylethanethiolate (PET), a hydrophobic ligand, was synthesized by a previously reported

method ( $\text{Au}_{25}(\text{PET})_{18}$ ; Fig. S2 and S3†).<sup>27,49</sup> The obtained  $\text{Au}_{25}(\text{PET})_{18}$  was dissolved in acetone and loaded on gCN using an impregnation method ( $\text{Au}_{25}(\text{PET})_{18}/\text{gCN}$ ). We characterized the prepared  $\text{Au}_{25}(\text{PET})_{18}/\text{gCN}$  using various methods (Fig. 2 and S4†). The transmission electron microscopy (TEM) image of  $\text{Au}_{25}(\text{PET})_{18}/\text{gCN}$  shown in Fig. 2a showed that the particle size of  $\text{Au}_{25}(\text{PET})_{18}$  cocatalysts on gCN (particle size:  $1.11 \pm 0.19$  nm) was almost the same as  $\text{Au}_{25}(\text{PET})_{18}$  before adsorption on gCN (particle size:  $1.03 \pm 0.13$  nm). Compared with the sizes of the Au NP cocatalysts of Au NP-loaded gCN (Au NP/gCN; particle size:  $6.55 \pm 1.35$  nm; Fig. 2c and S5†) prepared using the conventional PD method,  $\text{Au}_{25}(\text{PET})_{18}$  cocatalysts have smaller and monodispersed sizes. The Au L<sub>3</sub>-edge X-ray absorption near edge structure (XANES) spectra showed that (1) the  $\text{Au}_{25}(\text{PET})_{18}$  cocatalyst on gCN has a metallic electronic state and (2) the electronic state of  $\text{Au}_{25}(\text{PET})_{18}$  is maintained before and after adsorption on gCN (Fig. 3A and S4†). Such the change in the electronic state between the Au cocatalyst and gCN was not observed by XPS (Fig. S6†). The Au L<sub>3</sub>-edge Fourier transform

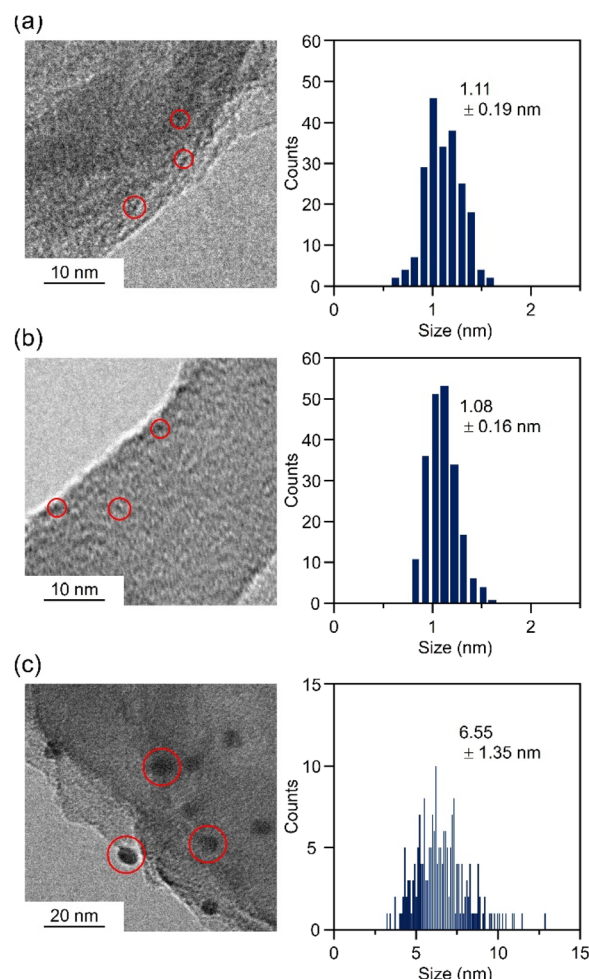


Fig. 2 TEM images and resulting histograms of the particle-size distribution for Au cocatalysts for (a)  $\text{Au}_{25}(\text{PET})_{18}/\text{gCN}$ , (b)  $\text{Au}_{25}(\text{PET}, \text{p-MBA})_{18}/\text{gCN}$  and (c) Au NP/gCN. Loading amounts of Au are 0.1, 0.1 and 3.0 wt% for  $\text{Au}_{25}(\text{PET})_{18}/\text{gCN}$ ,  $\text{Au}_{25}(\text{PET}, \text{p-MBA})_{18}/\text{gCN}$  and Au NP/gCN, respectively.



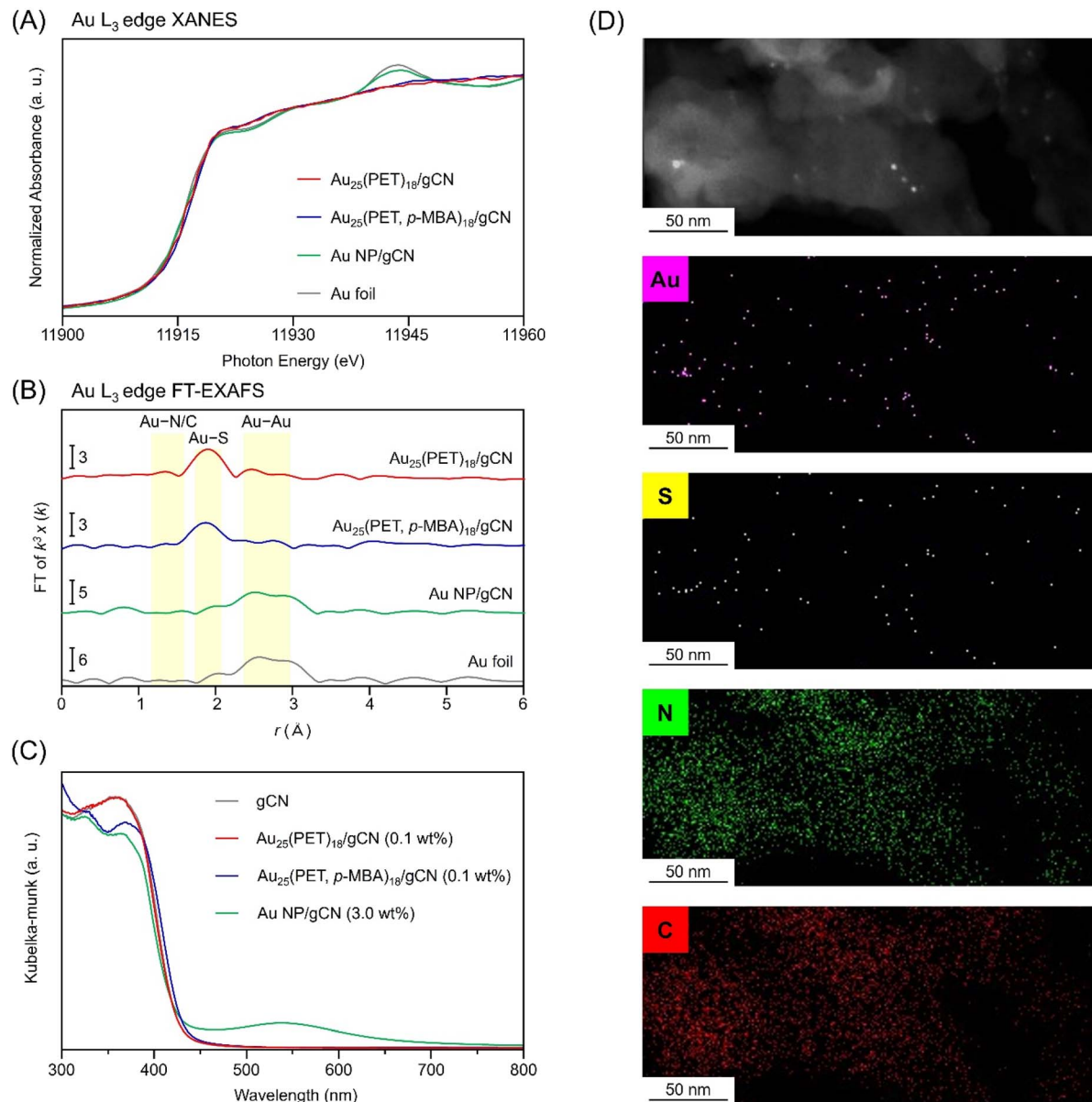


Fig. 3 Characterization of cocatalyst-loaded gCN photocatalysts. Au  $L_3$ -edge (A) XANES, (B) FT-EXAFS spectra and (C) DR spectra. (D) HAADF-STEM images and EDS elemental mapping of  $Au_{25}(PET)_{18}/gCN$  (Au–M, S–K, C–K and N–K). In (A and B), Au  $L_3$ -edge XANES and FT-EXAFS spectra of Au foil is also shown for comparison. In (B), the peaks at  $\approx 1.9$  and  $2.6\text{--}3.0$   $\text{\AA}$  are assigned to the Au–S and Au–Au bonds, respectively. Loading amounts of Au are 0.1, 0.1 and 3.0 wt% for  $Au_{25}(PET)_{18}/gCN$ ,  $Au_{25}(PET, p\text{-}MBA)_{18}/gCN$  and Au NP/gCN, respectively.

extended X-ray absorption fine structure (FT-EXAFS) spectra showed a peak ( $\approx 1.9$   $\text{\AA}$ ) due to the Au–S bond, suggesting that the SR ligands of  $Au_{25}(PET)_{18}$  remain even after adsorption and that their geometric structure is mostly maintained (Fig. 3B and S4†). In the DR spectrum, there is no strong absorption in the visible region due to localized surface plasmon resonance, as seen in Au NP formed by aggregation (Fig. 3C and S4†). In an energy dispersive X-ray spectroscopy (EDS) elemental mapping obtained using a high-angle annular dark field-scanning TEM (HAADF-STEM) (Fig. 3D), Au and S were mapped to the same location, confirming that  $Au_{25}(PET)_{18}$  cocatalyst was located on gCN. These analyses strongly indicated that  $Au_{25}(PET)_{18}$

cocatalyst was loaded on gCN while largely maintaining its geometric structure.

The photocatalytic CO<sub>2</sub>RR activity of the  $Au_{25}(PET)_{18}/gCN$  was evaluated using a reaction cell under CO<sub>2</sub> flow with light irradiation (Fig. 4). In the measurement, triisopropanolamine (TIPA) was added (20 vol%) as a hole sacrificial reagent to correctly evaluate the photocatalytic CO<sub>2</sub>RR activity.<sup>50</sup> The Au cocatalyst-loaded gCN was dispersed in water with the sacrificial agent, it was irradiated with visible light using a blue LED (405 nm), and H<sub>2</sub> or CO evolution was quantified using a gas chromatograph at regular time intervals (Fig. S7†). By analysing the reaction solution with a high-performance liquid

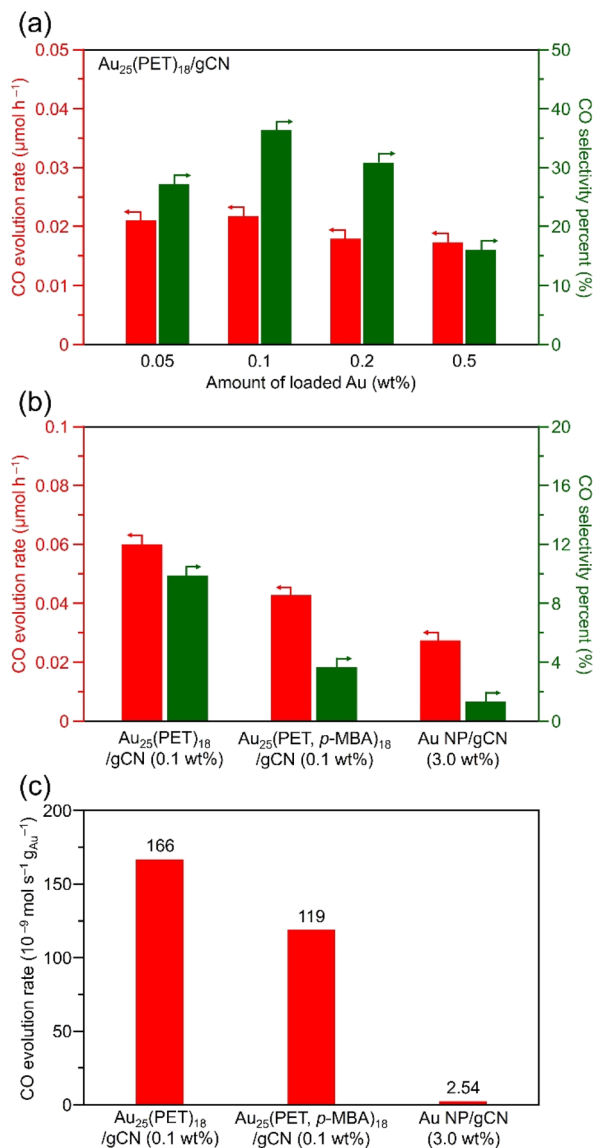


Fig. 4 Photocatalytic CO<sub>2</sub>RR activity of Au cocatalyst-loaded gCN photocatalysts. (a) Dependence on loading weight of Au for Au<sub>25</sub>(PET)<sub>18</sub>/gCN. (b) Comparisons of CO evolution rates and resulting CO selectivities and (c) CO evolution rates per loading weight of Au, for Au<sub>25</sub>(PET)<sub>18</sub>/gCN, Au<sub>25</sub>(PET, p-MBA)<sub>18</sub>/gCN and Au NP/gCN. Photocatalyst: 100 mg, solution: water (60 mL) with TIPA (12.5 g), flow gas: CO<sub>2</sub> (1 atm), light source: 405 nm LED lamp and cell: top-irradiation cell. In (b) and (c), loading weights of Au are 0.1, 0.1 and 3.0 wt% for Au<sub>25</sub>(PET)<sub>18</sub>/gCN, Au<sub>25</sub>(PET, p-MBA)<sub>18</sub>/gCN and Au NP/gCN, respectively.

chromatograph, it was confirmed that the product did not contain any liquid-phase CO<sub>2</sub>RR products. In addition, by evaluating the same measurement under Ar flow, it was confirmed that the obtained CO was derived from the flowing CO<sub>2</sub> (Fig. S8†).

For the photocatalytic CO<sub>2</sub>RR experiments, we first investigated the optimal Au-loading weights of Au<sub>25</sub>(PET)<sub>18</sub>/gCN. As a result, the highest CO evolution rate was obtained when the Au-loading weight was set to 0.1 wt% (Fig. 4a). Therefore, in the

subsequent experiments, we used Au<sub>25</sub>(PET)<sub>18</sub>/gCN prepared with this optimal 0.1 wt% of Au-loading weight.

Next, we investigated the effects of hydrophilic and hydrophobic ligands on Au<sub>25</sub> NC on the photocatalytic CO<sub>2</sub>RR activity. In our previous report, we have succeeded in improving the hydrophilicity of Au<sub>25</sub> NC by exchanging some of the ligands of Au<sub>25</sub>(PET)<sub>18</sub> with 4-mercaptopbenzoic acid (*p*-MBA), a hydrophilic ligand with a structure relatively similar to that of PET.<sup>27</sup> Accordingly, we prepared Au<sub>25</sub> NC in which some of the ligands were exchanged by *p*-MBA (Au<sub>25</sub>(PET, *p*-MBA)<sub>18</sub>; Fig. S2 and S3†), and loaded it on gCN by a liquid-phase adsorption method to prepare a photocatalyst (Au<sub>25</sub>(PET, *p*-MBA)<sub>18</sub>/gCN; Fig. 2b, 3 and S9†). The photocatalytic CO<sub>2</sub>RR activity of the obtained Au<sub>25</sub>(PET, *p*-MBA)<sub>18</sub>/gCN is shown in Fig. 4b. Interestingly, it was found that hydrophilic Au<sub>25</sub>(PET, *p*-MBA)<sub>18</sub>/gCN has 2.70 times lower CO selectivity (selectivity<sub>CO</sub> = 3.66%) than hydrophobic Au<sub>25</sub>(PET)<sub>18</sub>/gCN (selectivity<sub>CO</sub> = 9.87%). Jiang and Lee *et al.* reported that Au<sub>25</sub>(SR)<sub>18</sub> protected by a hydrophilic ligand (3-mercaptopropanoic acid or 3-mercaptop-1-propanesulfonic acid), which allowed efficient H<sup>+</sup> relay, had a higher electrochemical HER than hydrophobic 1-hexanethiolate (SC<sub>6</sub>) ligand-protected Au<sub>25</sub>(SC<sub>6</sub>)<sub>18</sub>.<sup>33</sup> In our study, the photocatalytic HER selectivity was also improved when hydrophilic Au<sub>25</sub>(PET, *p*-MBA)<sub>18</sub>/gCN was used, probably because *p*-MBA induced an effective H<sup>+</sup> relay. Although hydrophilic NC were used as cocatalysts in photocatalytic CO<sub>2</sub>RR in the previous report,<sup>51</sup> this study demonstrated that the use of these hydrophilic NC as cocatalysts (1) promoted the HER as a competing reaction and (2) thereby reduced the selectivity of the CO<sub>2</sub>RR (Fig. 4b and c).

Next, we compared the photocatalytic CO<sub>2</sub>RR activity between Au<sub>25</sub>(PET)<sub>18</sub>/gCN, which has a hydrophobic ligand suitable for photocatalytic CO<sub>2</sub>RR, and Au NP/gCN prepared using a conventional PD method (Fig. 4b). In this experiment, we also optimized the Au-loading weights of Au NP/gCN, which was found to be 3.0 wt% of Au (Fig. S10 and S11†). The results of the comparison for their photocatalytic CO<sub>2</sub>RR activity are also shown in Fig. 4b. The results demonstrated that (1) even though the Au-loading weight of Au<sub>25</sub>(PET)<sub>18</sub>/gCN was 30 times less than that of Au NP/gCN, Au<sub>25</sub>(PET)<sub>18</sub>/gCN shows higher CO evolution rate than Au NP/gCN (0.06 vs. 0.03 μmol<sub>CO</sub> h<sup>-1</sup>, Fig. 4b) and (2) Au<sub>25</sub>(PET)<sub>18</sub>/gCN shows a greatly suppressed H<sub>2</sub> evolution rate compared with Au NP/gCN (0.61 vs. 2.10 μmol<sub>H2</sub> h<sup>-1</sup>, Fig. 4b). Comparing the CO evolution rate per Au-loading weight in Fig. 4c, Au<sub>25</sub>(PET)<sub>18</sub>/gCN and Au<sub>25</sub>(PET, *p*-MBA)<sub>18</sub>/gCN showed 66 and 47 times higher CO evolution rates than Au NP/gCN, respectively (166 vs. 119 vs. 2.54 × 10<sup>-9</sup> mol s<sup>-1</sup> g<sub>Au</sub><sup>-1</sup>). Accordingly, Au<sub>25</sub>(PET)<sub>18</sub>/gCN showed the highest CO selectivity (9.87% vs. 3.66% vs. 1.31% for Au<sub>25</sub>(PET)<sub>18</sub>/gCN, Au<sub>25</sub>(PET, *p*-MBA)<sub>18</sub> and Au NP/gCN, respectively). The previous study<sup>38</sup> reported that Au<sub>25</sub>(SR)<sub>18</sub> has a suitable CO<sub>2</sub> adsorption site. Furthermore, molecular dynamics simulations suggested that the presence of hydrophilic ligands in [Au<sub>25</sub>(SR)<sub>18</sub>]<sup>-</sup> efficiently induced HER due to enhanced proton transfer facilitated by hydrogen bonds.<sup>52</sup> Therefore, it can be considered that Au<sub>25</sub>(PET)<sub>18</sub>/gCN promoted photocatalytic CO<sub>2</sub>RR with a relatively high CO selectivity because Au<sub>25</sub>(PET)<sub>18</sub>/gCN contains

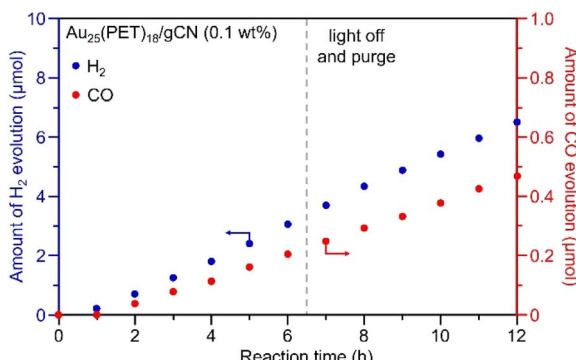


Fig. 5 Time dependence of photocatalytic CO<sub>2</sub>RR activity of Au<sub>25</sub>(PET)<sub>18</sub>/gCN. Photocatalyst: 100 mg, solution: water (60 mL) with TIPA (12.5 g), flow gas: CO<sub>2</sub> (1 atm), light source: 405 nm LED lamp and cell: top-irradiation cell. Loading weight of Au is 0.1 wt% for Au<sub>25</sub>(PET)<sub>18</sub>/gCN.

both the suitable CO<sub>2</sub> adsorption site and hydrophobic PET which leads to the suppression of HER.

Finally, we evaluated the catalytic stability of Au<sub>25</sub>(PET)<sub>18</sub>/gCN, which has a relatively good CO evolution rate and selectivity. In general, the excited electrons generated by the photocatalytic reaction have a strong reduction power and may reductively decompose many organic substances. Therefore, we measured the long-term photocatalytic CO<sub>2</sub>RR activity of Au<sub>25</sub>(PET)<sub>18</sub>/gCN to evaluate its durability. As a result, it was shown that Au<sub>25</sub>(PET)<sub>18</sub>/gCN stably produced CO and its selectivity did not change even after 12 h of visible-light irradiation (Fig. 5). We also investigated the size of the cocatalyst after the photocatalytic activity test using TEM. As a result, the particle size of the Au<sub>25</sub>(PET)<sub>18</sub> cocatalyst was almost the same as that of the Au<sub>25</sub>(PET)<sub>18</sub> just after loading on gCN (particle size: 1.11 ± 0.17 nm; Fig. S4A†). In fact, no change in the diffraction pattern due to Au aggregation was observed in the powder X-ray diffraction (Fig. S12†). Au L<sub>3</sub>-edge XANES spectra showed that the electronic state of the Au<sub>25</sub>(PET)<sub>18</sub> cocatalyst did not change significantly before and after light irradiation (Fig. S4C†). Furthermore, surprisingly, the peak ( $\approx$ 1.9 Å) derived from the Au–S bond was maintained in the Au L<sub>3</sub>-edge FT-EXAFS spectrum even after the evaluation of photocatalytic CO<sub>2</sub>RR activity (Fig. S4D†), suggesting that most of the ligands remain undecomposed even after long-term light irradiation. These results revealed that Au<sub>25</sub>(PET)<sub>18</sub>/gCN, which has a strong Au–S bond, has high stability against light irradiation.

## Conclusions

The loading of metal NC cocatalysts leads to a significant improvement in photocatalytic activity. In this study, we investigated the effect of organic ligands protecting the surface of these metal NC cocatalysts on the activity and selectivity of photocatalytic CO<sub>2</sub>RR. The results demonstrated that (1) the introduction of hydrophilic ligands to the Au<sub>25</sub> NC cocatalyst promotes the competing HER, whereas (2) the introduction of hydrophobic ligands to the Au<sub>25</sub> NC cocatalyst suppresses the

HER, leading to the progress of photocatalytic CO<sub>2</sub>RR with relatively high CO selectivity. In this way, although it has been generally believed that the presence of organic ligands on the metal NC surface reduces photocatalytic activity, this study revealed that the presence of hydrophobic ligands effectively suppresses the competing HER in photocatalytic CO<sub>2</sub>RR. Furthermore, it was found that the hydrophobic Au<sub>25</sub>(PET)<sub>18</sub>-loaded photocatalysts show a 66 times higher CO evolution rate per Au-loading weight and relatively high CO selectivity compared with Au NP-loaded photocatalysts. These results will provide clear design guidelines for achieving high-performance photocatalytic CO<sub>2</sub>RR by loading metal NC cocatalysts. In the future, it is expected that the obtained knowledge will be applied to a semiconductor photocatalyst suitable for photocatalytic CO<sub>2</sub>RR<sup>17</sup> to create high-performance CO<sub>2</sub>RR photocatalysts with significantly improved selectivity and activity, which will contribute to practical use (Fig. S13†).

## Data availability

All data generated in this study are provided in the manuscript and ESI.†

## Author contributions

T. K. and Y. N. conceived the research and designed the experiments. Y. Y., Y. T., and T. K. performed the syntheses, characterization and measurements of the CO<sub>2</sub>RR activity. T. K. and Y. N. wrote the manuscript.

## Conflicts of interest

There are no conflicts to declare.

## Acknowledgements

The authors thank Mr Kengo Nagatsuka, Dr Yuichi Yamaguchi and Prof. Akihiko Kudo (Tokyo University of Science) for technical assistance. This work was supported by the Japan Society for the Promotion of Science (JSPS) KAKENHI (grant numbers 23H00289, 22K19012 and 24K01459). Funding from the Carbon Recycling Fund Institute, the Japan Gas Association, the Iwatani Naoji Foundation, the Ichimura Foundation for New Technology, the Suzuki Foundation, and the Japan Keirin Autorace Foundation is gratefully acknowledged.

## Notes and references

- 1 J. L. White, M. F. Baruch, J. E. Pander III, Y. Hu, I. C. Fortmeyer, J. E. Park, T. Zhang, K. Liao, J. Gu, Y. Yan, T. W. Shaw, E. Abelev and A. B. Bocarsly, *Chem. Rev.*, 2015, **115**, 12888–12935.
- 2 X. Li, J. Yu, M. Jaroniec and X. Chen, *Chem. Rev.*, 2019, **119**, 3962–4179.
- 3 A. Kudo and Y. Miseki, *Chem. Soc. Rev.*, 2009, **38**, 253–278.
- 4 B. A. Pinaud, J. D. Benck, L. C. Seitz, A. J. Forman, Z. Chen, T. G. Deutsch, B. D. James, K. N. Baum, G. N. Baum,



S. Ardo, H. Wang, E. Miller and T. F. Jaramillo, *Energy Environ. Sci.*, 2013, **6**, 1983–2002.

5 Y. Wang, H. Suzuki, J. Xie, O. Tomita, D. J. Martin, M. Higashi, D. Kong, R. Abe and J. Tang, *Chem. Rev.*, 2018, **118**, 5201–5241.

6 D. M. Fabian, S. Hu, N. Singh, F. A. Houle, T. Hisatomi, K. Domen, F. E. Osterloh and S. Ardo, *Energy Environ. Sci.*, 2015, **8**, 2825–2850.

7 Q. Wang and K. Domen, *Chem. Rev.*, 2020, **120**, 919–985.

8 K. Iizuka, T. Wato, Y. Miseki, K. Saito and A. Kudo, *J. Am. Chem. Soc.*, 2011, **133**, 20863–20868.

9 K. Teramura, Z. Wang, S. Hosokawa, Y. Sakata and T. Tanaka, *Chem.-Eur. J.*, 2014, **20**, 9906–9909.

10 K. Teramura and T. Tanaka, *Phys. Chem. Chem. Phys.*, 2018, **20**, 8423–8431.

11 S. Yoshino, T. Takayama, Y. Yamaguchi, A. Iwase and A. Kudo, *Acc. Chem. Res.*, 2022, **55**, 966–977.

12 M. Yamamoto, T. Yoshida, N. Yamamoto, T. Nomoto, Y. Yamamoto, S. Yagi and H. Yoshida, *J. Mater. Chem. A*, 2015, **3**, 16810–16816.

13 Y. Jiang, Y. Yu, X. Zhang, M. Weinert, X. Song, J. Ai, L. Han and H. Fei, *Angew. Chem., Int. Ed.*, 2021, **60**, 17388–17393.

14 T. Kawakaki, Y. Akinaga, D. Yazaki, H. Kameko, D. Hirayama and Y. Negishi, *Chem.-Eur. J.*, 2023, **29**, e202203387.

15 J. Ran, M. Jaroniec and S.-Z. Qiao, *Adv. Mater.*, 2018, **30**, 1704649.

16 S. N. Habisreutinger, L. Schmidt-Mende and J. K. Stolarczyk, *Angew. Chem., Int. Ed.*, 2013, **52**, 7372–7408.

17 W. Soontornchaiyakul, S. Yoshino, T. Kanazawa, R. Haruki, D. Fan, S. Nozawa, Y. Yamaguchi and A. Kudo, *J. Am. Chem. Soc.*, 2023, **145**, 20485–20491.

18 Q. Yao, T. Chen, X. Yuan and J. Xie, *Acc. Chem. Res.*, 2018, **51**, 1338–1348.

19 N. A. Sakthivel and A. Dass, *Acc. Chem. Res.*, 2018, **51**, 1774–1783.

20 Z. Gan, N. Xia and Z. Wu, *Acc. Chem. Res.*, 2018, **51**, 2774–2783.

21 A. Ghosh, O. F. Mohammed and O. M. Bakr, *Acc. Chem. Res.*, 2018, **51**, 3094–3103.

22 J. Yan, B. K. Teo and N. Zheng, *Acc. Chem. Res.*, 2018, **51**, 3084–3093.

23 I. Chakraborty and T. Pradeep, *Chem. Rev.*, 2017, **117**, 8208–8271.

24 Y. Du, H. Sheng, D. Astruc and M. Zhu, *Chem. Rev.*, 2020, **120**, 526–622.

25 A. Fernando, K. L. D. M. Weerawardene, N. V. Karimova and C. M. Aikens, *Chem. Rev.*, 2015, **115**, 6112–6216.

26 D. Hirayama, T. Kawakaki, S. Oguchi, M. Ogano, N. Kon, T. Yasuda, A. Higami and Y. Negishi, *J. Am. Chem. Soc.*, 2024, **146**, 26808–26818.

27 T. Kawakaki, Y. Kataoka, M. Hirata, Y. Akinaga, R. Takahata, K. Wakamatsu, Y. Fujiki, M. Kataoka, S. Kikkawa, A. S. Alotabi, S. Hossain, D. J. Osborn, T. Teranishi, G. G. Andersson, G. F. Metha, S. Yamazoe and Y. Negishi, *Angew. Chem., Int. Ed.*, 2021, **60**, 21340–21350.

28 T. Kawakaki, M. Kawachi, D. Yazaki, Y. Akinaga, D. Hirayama and Y. Negishi, *Nanomaterials*, 2022, **12**, 344.

29 D. Yazaki, T. Kawakaki, D. Hirayama, M. Kawachi, K. Kato, S. Oguchi, Y. Yamaguchi, S. Kikkawa, Y. Ueki, S. Hossain, D. J. Osborn, F. Ozaki, S. Tanaka, J. Yoshinobu, G. F. Metha, S. Yamazoe, A. Kudo, A. Yamakata and Y. Negishi, *Small*, 2023, **19**, 2208287.

30 C. M. Pelicano, M. Saruyama, R. Takahata, R. Sato, Y. Kitahama, H. Matsuzaki, T. Yamada, T. Hisatomi, K. Domen and T. Teranishi, *Adv. Funct. Mater.*, 2022, **32**, 2202987.

31 H. Wang, X. Zhang, W. Zhang, M. Zhou and H.-L. Jiang, *Angew. Chem., Int. Ed.*, 2024, **63**, e202401443.

32 A. S. Alotabi, D. J. Osborn, S. Ozaki, Y. Kataoka, Y. Negishi, S. Tesana, G. F. Metha and G. G. Andersson, *Mater. Adv.*, 2022, **3**, 3620–3630.

33 K. Kwak, W. Choi, Q. Tang, D.-e. Jiang and D. Lee, *J. Mater. Chem. A*, 2018, **6**, 19495–19501.

34 Y. Negishi, M. Mizuno, M. Hirayama, M. Omatoi, T. Takayama, A. Iwase and A. Kudo, *Nanoscale*, 2013, **5**, 7188–7192.

35 M. Zhu, C. M. Aikens, F. J. Hollander, G. C. Schatz and R. Jin, *J. Am. Chem. Soc.*, 2008, **130**, 5883–5885.

36 M. W. Heaven, A. Dass, P. S. White, K. M. Holt and R. W. Murray, *J. Am. Chem. Soc.*, 2008, **130**, 3754–3755.

37 T. Kawakaki, T. Okada, D. Hirayama and Y. Negishi, *Green Chem.*, 2024, **26**, 122–163.

38 D. R. Kauffman, D. Alfonso, C. Matranga, H. Qian and R. Jin, *J. Am. Chem. Soc.*, 2012, **134**, 10237–10243.

39 D. R. Kauffman, J. Thakkar, R. Siva, C. Matranga, P. R. Ohodnicki, C. Zeng and R. Jin, *ACS Appl. Mater. Interfaces*, 2015, **7**, 15626–15632.

40 H. Seong, V. Efremov, G. Park, H. Kim, J. S. Yoo and D. Lee, *Angew. Chem., Int. Ed.*, 2021, **60**, 14563–14570.

41 W.-J. Ong, L.-L. Tan, Y. H. Ng, S.-T. Yong and S.-P. Chai, *Chem. Rev.*, 2016, **116**, 7159–7329.

42 Y. Wang, X. Wang and M. Antonietti, *Angew. Chem., Int. Ed.*, 2012, **51**, 68–89.

43 Z. Zhao, Y. Sun and F. Dong, *Nanoscale*, 2015, **7**, 15–37.

44 Y. Zhu, T. Wang, T. Xu, Y. Li and C. Wang, *Appl. Surf. Sci.*, 2019, **464**, 36–42.

45 S. Cao, J. Low, J. Yu and M. Jaroniec, *Adv. Mater.*, 2015, **27**, 2150–2176.

46 Q. Lu, K. Eid, W. Li, A. M. Abdullah, G. Xu and R. S. Varma, *Green Chem.*, 2021, **23**, 5394–5428.

47 J. Lin, W. Tian, H. Zhang, X. Duan, H. Sun and S. Wang, *Energy Fuels*, 2021, **35**, 7–24.

48 Y. Zhou, Z. Wang, L. Huang, S. Zaman, K. Lei, T. Yue, Z. a. Li, B. You and B. Y. Xia, *Adv. Energy Mater.*, 2021, **11**, 2003159.

49 H. Qian, C. Liu and R. Jin, *Sci. China:Chem.*, 2012, **55**, 2359–2365.

50 P. Zhang, T. Sun, L. Xu, Q. Xu, D. Wang, W. Liu, T. Zheng, G. Yang and J. Jiang, *ACS Sustainable Chem. Eng.*, 2023, **11**, 343–352.

51 L. Tian, Y. Luo, K. Chu, D. Wu, J. Shi and Z. Liang, *Chem. Commun.*, 2019, **55**, 12976–12979.

52 L. Luo, X. Zhou, Y. Chen, F. Sun, L. Wang and Q. Tang, *Chem. Sci.*, 2025, DOI: [10.1039/D4SC07181F](https://doi.org/10.1039/D4SC07181F).

